DOI 10.4430/bgo00392

Thin-bed reservoir characterisation by integration of seismic inversion, multi attributes analysis and neural network: a case study in the Sufyan oil field of the Muglad rift basin, Sudan

M.E.K. Shuaib[1,2] and M.C. Berguig[2]

[1] *Department of Geology, Faculty of Science, University of Khartoum, Khartoum, Sudan*
[2] *Faculty of Earth Sciences, Geography and Territorial Planning, University of Science and Technology Houari Boumediene, Algiers, Algeria*

(Received: 13 September 2021; accepted: 11 April 2022; published online: 23 June 2022)

ABSTRACT This study is a comparative analysis of three types of post-stack inversion techniques, namely, Band-Limited (BLI), Linear Programming Sparse-Spike (LP-SSI), along with Model-Based (MBI), in addition to a neural network in the Sufyan oil field of the Muglad rift basin, Sudan. It investigates whether a combination of multi-attribute analysis and a neural network could bring about a better definition of unresolved thin reservoir layers. Applied inversion techniques produce accurate and reliable results, while the MBI method brings a higher correlation coefficient (0.988) and higher amplitude spectrum correlation (0.999). Hence, it is better for the Sufyan seismic data. The resulting resolution and precision of multi-attribute rock properties prediction is achieved using multi-layer feed forward neural (MLFN), probabilistic neural (PNN), along with radial basis function neural (RBFN) networks to predict porosity. The combination of PNN and LP-SSI has the highest training correlation of 0.9534 and validation correlation of 0.7998. However, MLFN shows that LP-SSI, when used as an external attribute, produces high-resolution images compared to those estimated with other combinations with training correlation of 0.9400 and validation correlation of 0.7111. The resulting resolution and precision in terms of porosities are higher when the combination of LP-SSI and MLFN approach is used compared to that estimated by other methods. Thus, LP-SSI is more accurate than other techniques to predict petrophysical parameters in the Sufyan oil field.

Key words: Sufyan sub-basin, Muglad basin, seismic inversion, multi-attribute, neural network, porosity, thin beds, reservoir characterisation, Sudan.

1. Introduction

In the Muglad rift basin, several Cretaceous formations have produced good quantities of oil during the past decades. The Abu Gabra Formation sandstone strata are considered a prominent objective within the northern region of the basin yet a high degree of heterogeneity is encountered (Makeen *et al.*, 2016; Yassin *et al.*, 2018). These strata have thicknesses, which are more or less adequate to the temporal resolution of seismic information with respect to the dominant frequencies commonly obtained in the data. Hence, it is difficult to resolve unconnected reflections from the tops and bottoms of such layers.

Recent papers on the Abu Gabra Formation in the Muglad basin generally focus on

© 2022 - OGS

palynological studies (Cole *et al.*, 2017), source rock characterisation and evaluation (Makeen *et al.*, 2015a, 2015b, 2015c), as well as tectonostratigraphy and sedimentology (Wu *et al.*, 2015). Yassin *et al.* (2017) used gravity and seismic data to compile the evolutionary history of the Sufyan sub-basin and its contribution in hydrocarbon formation. Makeen *et al.* (2016) studied the upper Abu Gabra sandstones with emphasis on sedimentology, diagenesis, and reservoir quality. Yassin *et al.* (2018) studied the facies, depositional environments, sequence stratigraphy and also diagenesis, in addition to its relation to the quality of the reservoir within the sandstone of the Lower Cretaceous of the formation.

Apart from reservoir heterogeneity, comprehensive studies in the Early Cretaceous Abu Gabra Formation sandstones are scarce. The application of seismic multi-attribute analysis and artificial intelligence technologies for reservoir property and heterogeneity predictions in Sudan oil fields are relatively rare, and generally in the form of short notes, abstracts and internal technical reports.

Today, the main challenge in the problem of reservoir characterisation is how to combine various types of data in order to produce a precise, high resolution reservoir model. The technique of seismic multi-attribute transform is commonly practiced for extrapolating the physical properties of well records to seismic volumes, utilising seismic properties and well records (Hampson *et al.*, 2001). The approach adopted in this paper is the application of seismic attributes for exploration, characterisation, and reservoir development, which is similar to several published studies, such as Taner *et al.* (1979), Brown (1996, 2001), Gastaldi *et al.* (1997), Hampson *et al.* (2001), Sukmono (2007), Pavanel *et al.* (2009), Eftekharifar and Han (2011), and Shuaib (2013). However, the applied approach is used for thin-beds occurring below detection limit. Combined with the huge size of the data sets to be solved, these problems entail complicated issues that conventional methods cannot solve easily. Other methods of computation, such as artificial neural networks, have enabled analysis of data, allowing us to cope with inaccuracies and partial truths (Pandey *et al.*, 2020). Also, comparative studies with the same methodology regarding reservoir exploration, characterisation and development, are reported in the literature. In this study, however, the same approach is used for below detection limit thin-beds.

For many thin-bed reservoir studies (Widess, 1973), the determination of the presence and lateral extension of the thin beds themselves is the most important issue. Simm (2009) suggested different methods for defining thin layers, which have restrictions and require presumptions, which may not always be correct. According to Roden *et al.* (2017), the multi-attribute approach using self-organizing maps (SOM) of seismic property of below detection limit thin layers, can enhance their intervals delineation. Mora *et al.* (2020), use multi-attribute analysis and bandwidth extension for reservoir characterisation of thin sands, which improve unresolved thin-bed sand intervals.

This study follows a comparative analysis of three kinds of post-stack inversion techniques, namely Band-Limited (BLI), Linear Programming Sparse-Spike (LP-SSI), and Model-Based (MBI) inversions. It also employs three kinds of neural network namely: multi-layer feed forward neural (MLFN), probabilistic neural (PNN) along with radial basis function neural (RBFN) networks. It investigates which combination of attributes and neural network could result in a better definition of unresolved thin layers.

Furthermore, the study makes a precise interwell estimation of reservoir properties (porosity) and images thin beds that go beyond amplitude and impedance scaling but also produce consistent and more accurate results for Early Cretaceous sandstones of the Upper Abu Gabra Formation.

The study results will assist in understanding reservoir heterogeneities, provide a basis to fulfill various aspects regarding the reservoir in terms of high-resolution and will lead to reservoir

quality prediction. Subsequently, it will contribute to improving the hydrocarbon yield, long term management plans, and decision making.

2. Geological overview

The Muglad basin is the largest graben structure straddling the Sudan and South Sudan border. The total area of the basin is approximately 120,000 km^2 extending 800 km in an NW-SE direction with a maximum width of 200 km (Fig. 1a). The basin comprises eight sub-basins oriented in a NW-SE to NNW-SSE direction with extensional and strike-slip structural histories (Fig. 1b). Schull (1988) and Kaska (1989) have pointed out the presence of probably more than 16,000-m thickness of non-marine Cretaceous-Cenozoic sediments in the deepest parts.

A few wells in the Muglad basin reveal a succession that comprises thick claystones, fluvio-lacustrine sandstones, along with siltstones layers of Lower Cretaceous to Paleogene and Neogene age (Schull, 1988). The Muglad basin terminates at the NW by the strike of Central African Shear Zone (CASZ) (Fairhead, 1988).

Three major rift cycles mark the structural development of the basin; each is characterised

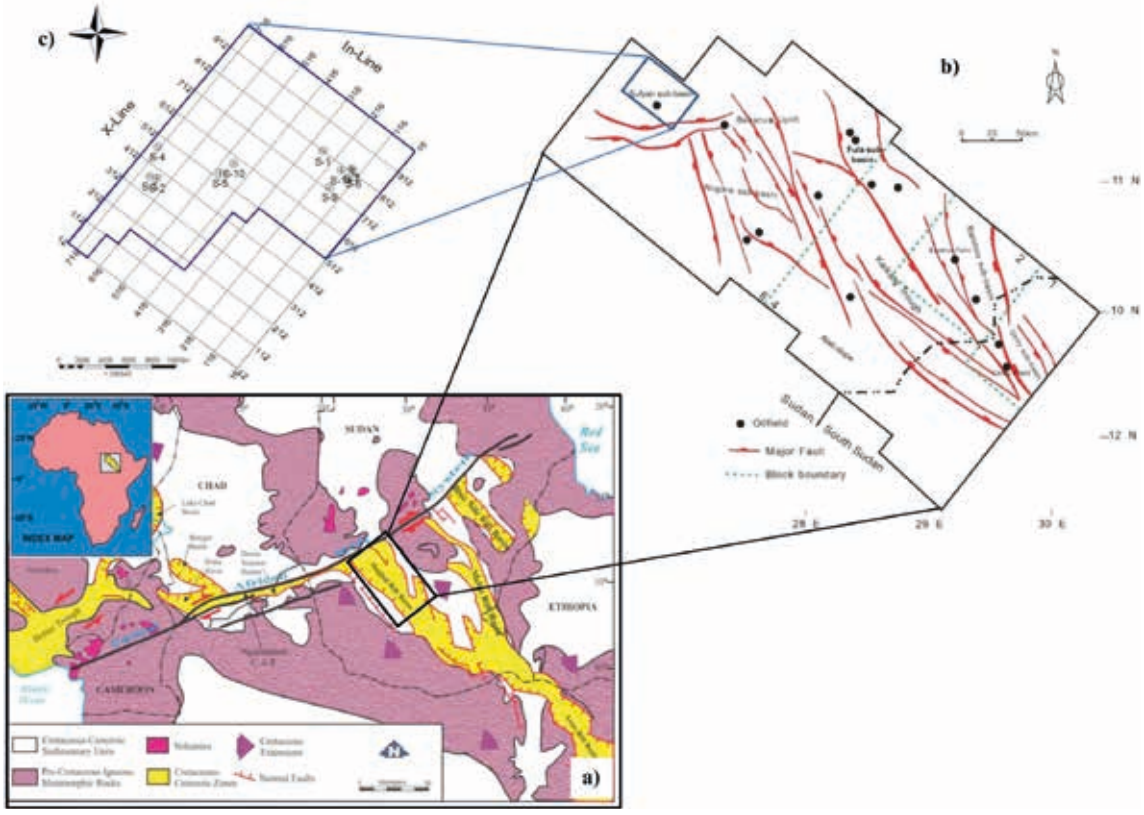

Fig. 1 - The study location area within the Muglad rift basin: a) distribution of rift basins within interior Sudan and their relation with CASZ (modified after Fairhead, 1988); b) illustration of the main structures of the northern and central part of the Muglad rift basin and the location of the sub-basin of Sufyan (modified from Lirong *et al.*, 2013); c) well locations and 3D seismic data in the Sufyan oil field used in the study. The blue line indicates the limits of seismic data area.

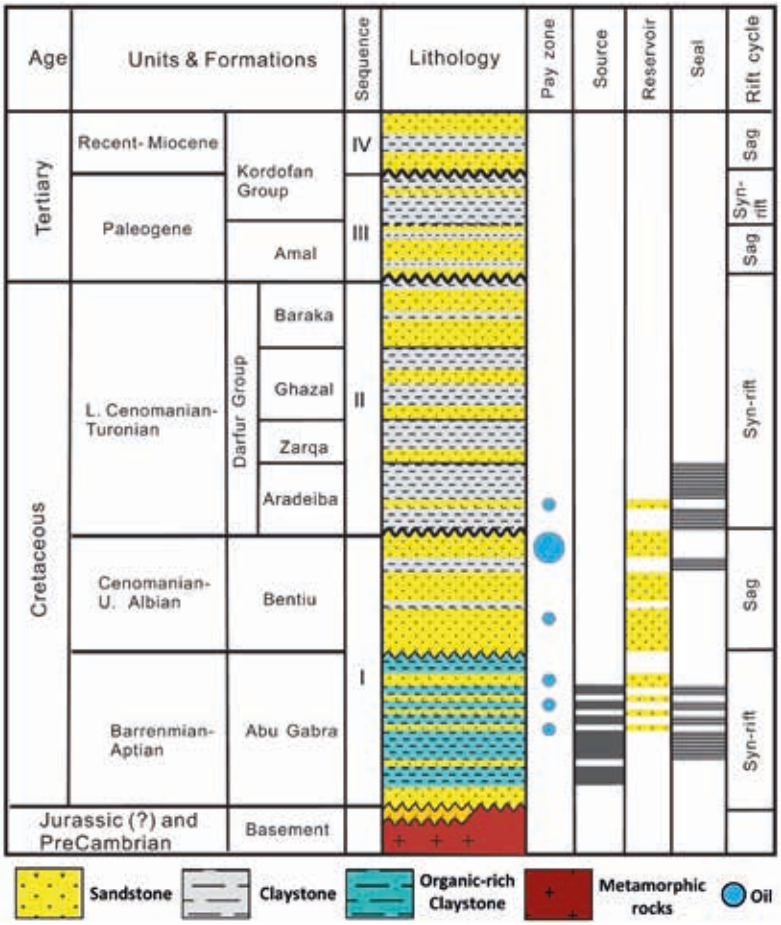

Fig. 2 - Muglad rift basin generalised stratigraphic column (modified from Schull, 1988; McHargue *et al.*, 1992; Tong *et al.*, 2004) indicating lithological units of seal source and reservoir, and the outline of the 3 stages of syn-rift referenced in the text.

by clastic sediments in coarsening-upward sequences (Schull, 1988). Exploratory drilling in the Muglad basin began in 1977 (Schull, 1988), and the first oil was discovered in the basin in May 1978.

This study was conducted in the Sufyan field, which lies within the NW of Muglad basin (Fig. 1b). Based on sedimentological evidence, seismic and log interpretations, Schull (1988) subdivided the Muglad succession into twelve formations (Fig. 2). In general, the Abu Gabra Formation is described as the major source rock, while the Bentiu Formation strata contain enormous hydrocarbon pools throughout the sub-basin. The mudstone of Darfur group (Senonian-Turonian) is described as a regional caprock all through the basin (Schull, 1988).

According to differences in lithology, the Abu Gabra Formation is split into three parts: AG3 at the bottom, AG2 in the middle, and AG1 at the top. The AG1 member is composed of light grey sandstone and grey mudstone of delta facies. The grains are coarsening-upwards. The top is medium-coarse grained sandstone with medium to poor porosity, and good roundness. Consequently, the AG1 member is considered as the main pay zone in Sufyan oil field, and has an unconformable contact with the superjacent Bentiu. This is the zone of interest for this study.

3. Materials and methods

For this study, data sets were acquired from the Sudan Ministry of Oil and Gas. The data comprises the following (Fig. 1c):

1. seismic cube of Post Stack Time Migration (PSTM): 3D seismic data of Sufyan sub-basin/ Muglad basin, representing an area of about 699 km^2 acquired in 2013 with a bin size of 25×25 m^2, record length of 6-s 2-way travel time (TWTT), 4-ms sampling rate, with the dominant frequency 15-20 Hz, and frequency range between 0-45 Hz;
2. ten well logs data: merged logs comprise gamma ray (GR), density log (ZDEN), neutron log (NPHI), along with acoustic log (DT) among others.

The approach adopted in this study can be divided into four primary parts: petrophysical analysis, seismic inversion, multi-attribute transforms, and artificial neural network application. Individual parts are outlined and discussed in the following sections and are provided in the flowchart in Fig. 3.

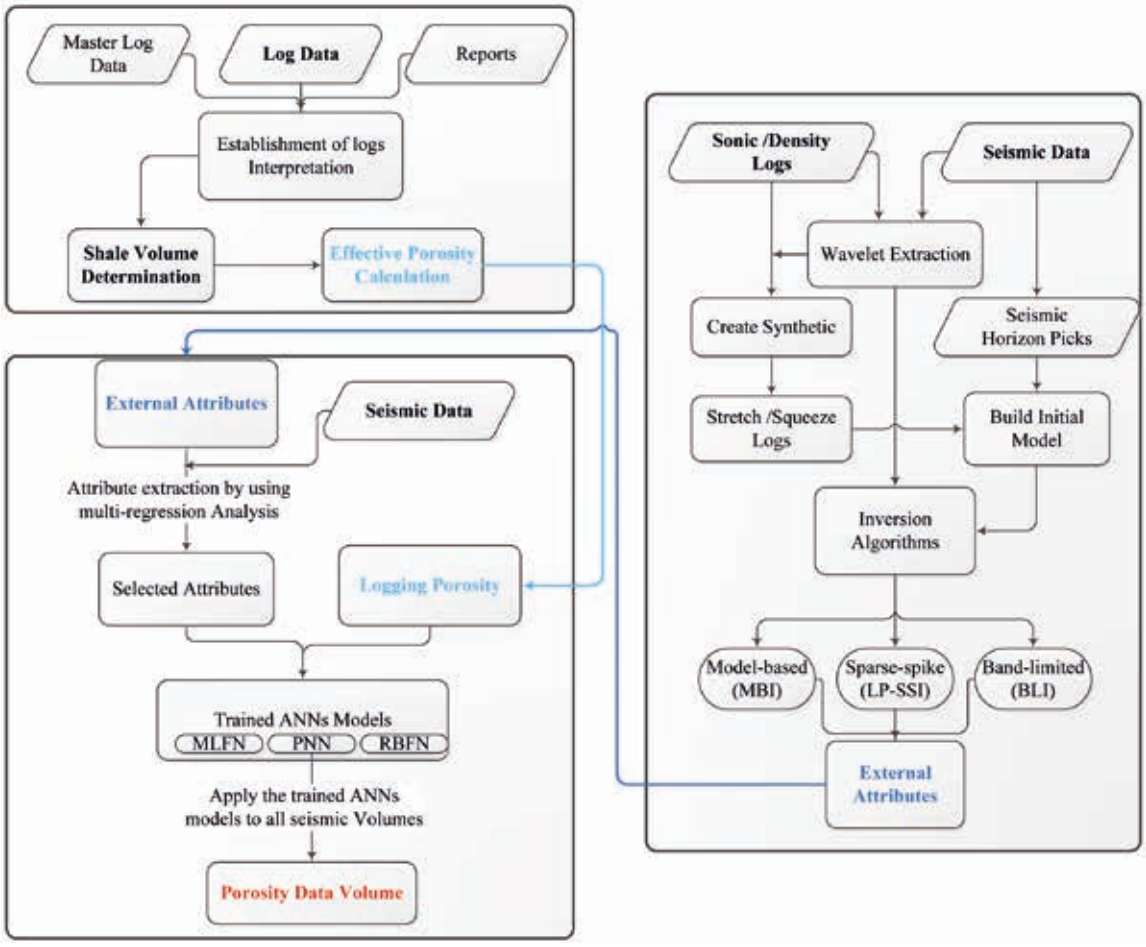

Fig. 3 - Study procedure flow chart and methodology.

3.1. Petrophysical analysis

In this section, interpreted petrophysical data sets of shale volume and porosity for each of the 10 wells are used as input in further steps for multi-attribute analysis and neural network application. Fig. 3 shows the procedures followed in this part:

- the shale index is defined from gamma ray (GR_{Index}) as:

$$GR_{Index} = \frac{GR_{log} - GR_{min}}{GR_{max} - GR_{min}} \quad (1)$$

where GR_{log} stands for gamma ray value read from log, GR_{min} stands for gamma ray value at the sand line; GR_{max} stands for gamma ray value at the shale line. A number of researchers have empirically correlated GR_{Index} to fractional volumes of shale relying upon age of formation, which resulted in linear and nonlinear relations. For shale volume (V_{Sh}) calculation, the equation of Larionov (1969) for older rocks was used (Schlumberger, 1987):

$$V_{Sh} = 0.33 \times (2^{GR_{Index}} - 1) \quad (2)$$

- effective porosity is obtained based on density-neutron combination by introducing the shale volume percentage into the equations. Based on neutron tool response, the neutron porosity is estimated. Moreover, the Dresser Atlas (1979) formula is used to determine density porosity for shaly formations (Carcione *et al.*, 2020) in the form:

$$\varphi_{D\_C} = \left[\frac{\rho_{ma} - \rho_b}{\rho_{ma} - \rho_f}\right] - V_{Sh}\left[\frac{\rho_{ma} - \rho_{sh}}{\rho_{ma} - \rho_f}\right] \quad (3)$$

where φ_{D_C} refers to shale free porosity of density, ρ_b is the measured density, ρ_{ma} is the density of the matrix, ρ_f is fluid average density, ρ_{sh} is the shale zone density. Then, shale free combined neutron and density porosity is calculated using the following formula (Schlumberger, 1987):

$$\varphi_{e_{(D-N)}} = \sqrt{\frac{\varphi_{D\_C}^2 + \varphi_{N\_C}^2}{2}} \quad (4)$$

where φ_{N_c} is the corrected neutron porosity = $\varphi_{N\_log} - V_{Sh}\,\varphi_{NSh}$, φ_{NSh} is the neutron porosity in adjacent shale, φ_{N_log} is measured neutron porosity.

3.2. Post-stacked seismic inversion

The seismic acoustic impedance inversion approach is becoming an increasingly important tool for carrying out reservoir prediction in oil exploration and development. It has higher accuracy in the lateral description of the fluid and lithology of the reservoir (Eskandari *et al.*,

2004; Maurya and Singh, 2015).

This approach will, in general, filter out the signature of wavelets from the seismic data, broadening the frequency band of inversion results that maximises resolution in both vertical and horizontal directions. It will also extend resolution beyond the seismic band, and minimises tuning effects (Russell, 1988; Russell and Hampson, 1991; Zhou, 2014).

Utilising three common post-stack seismic inversion methods, namely MBI, LP-SSI, along with BLI is the objective of this part of the work. On comparing their results, it is possible to decide which inversion most suits the Sufyan oil field. The inversion results will be further used as external attributes to ascertain both reservoir stratigraphy and property.

The key use of post-stack inversion is to reverse seismic trace $s(t)$ to get zero offset ground reflectivity expressed as a time series $r(t)$. Utilising $r(t)$, layer properties (i.e. acoustic impedance) is one of the rock-physics parameters, which can be obtained:

$$s(t) = w(t) * r(t) + n(t) \tag{5}$$

where $w(t)$ refers to seismic wavelet (assumed to be constant), $n(t)$ is additive noise, and * implies convolution.

Acoustic impedance is influenced by the type of lithology, porosity, fluid content, depth, pressure, and temperature. This gives a more efficient description of the subsurface than the extracted geological section from seismic data:

$$r_i = \frac{\rho_{i+1}V_{i+1} - \rho_i V_i}{\rho_{i+1}V_{i+1} + \rho_i V_i} = \frac{Z_{i+1} - Z_i}{Z_{i+1} + Z_i} \tag{6}$$

where r is the reflectivity (also called reflection coefficient series), ρ is the density, V is the velocity of P-wave, Z is the acoustic impedance.

The general flowchart of seismic inversion methods is shown in Fig. 3.

The reliability of the results is determined via two methods. Firstly, by extracting and comparing amplitude spectra of the seismic data and the synthetic seismic data generated by the algorithms. Secondly, by a cross-validation process, which is performed by systematically dropping a well completely from the initial model, performing the inversion at that location, and comparing the result with the hidden well.

The theory and application steps of BLI can be found in the literature (e.g. Waters, 1978; Russell, 1988; Ferguson and Margrave, 1996). For LP-SSI, its theory and application is described in Sacchi and Ulrych (1995), Ferguson and Margrave (1996), and Li (2001). Regarding MBI, the theory and work flow is illustrated in Russell (1988), Ferguson and Margrave (1996), and Maurya and Sarkar (2016).

3.3. Multi-attribute transform

The most common technique for the computation of seismic attributes involves extracting data from seismic information by direct or indirect computations and setting up a relationship with information of wells.

Reservoir rock properties were studied and predicted in many geoscience applications. For example, Hampson *et al.* (2001) statistical multi-attribute transform approach predicts log data from 3D seismic data. The method combines well information with multiple 3D or

2D seismic attributes through a statistical generalised linear regression approach using linear matrix theory:

$$L(t) = w_0 + w_1 * A_1(t) + w_2 * A_2(t) + w_3 * A_3(t) \quad (7)$$

where $L(t)$ refers to the desired rock property to be predicted, $w_i(t)$ are the unknown weights, and $A_i(t)$ are the seismic attribute values.

The steps below are followed to predict reservoir properties (Fig. 3):

1. use sample-based methodology to extract the attributes from the calibrated seismic traces with well-logs after converting them to time domain from their original depth domain;
2. compute acceptable statistical relationships for all well locations between reservoir porosity and extracted seismic attributes;
3. use the computed statistical relationship to predict the reservoir property (i.e. porosity) through multivariate regression (Hampson *et al.*, 2001);
4. use a cross-validation approach to check the derived relationship reliability.

3.4. Artificial Neural Network application

Multi-attribute transform examines the linear and nonlinear transform for both or either of two variables (target and attributes), in order to obtain the best fit line of the transformed data. Artificial Neural Networks (ANNs) is a nonlinear function to derive a relationship that can hold a larger dynamic range and high frequency.

Combination of extracted seismic attributes from seismic data via statistical methods along with artificial intelligent systems are used in characterising reservoirs in terms of lithology, prediction of hydrocarbon potentiality, and estimation of reservoir properties (e.g. Khoshdel and Riahi, 2011; Hou *et al.*, 2016; Maurya and Singh, 2018, 2019; Zahmatkesh *et al.*, 2018).

In this section, the relative performance of three ANN techniques is assessed. Multi-Layer Feed forward Neural network (MLFN), Probabilistic Neural Network (PNN), along with Radial Basis Function Neural network (RBFN) are used for porosity prediction to achieve better resolution enhancement for thin layers. To attain this goal the steps below are followed (Fig. 3):

1. appropriate attributes are selected by applying the stepwise regression (the same attribute list used in multi-attribute transform);
2. after neural network exercise (i.e. training), a relationship at well locations is derived;
3. trial and error analyses are performed and the best parameters giving the best estimated correlation coefficient (R^2) can be chosen;
4. cross-validation process is applied in order to check the reliability of the derived relationship.

4. Data analysis and results

4.1. Petrophysical analysis

The shale volume (V_{Sh}) was computed using Eqs. 1 and 2, following the picking of shale and sand lines. The density and neutron logs were used to compute porosity, which is believed to be total porosity (PHIT). In order to get effective porosity (PHIE), the density - neutron cross-plot using Eqs. 3 and 4 was used for correcting the porosity.

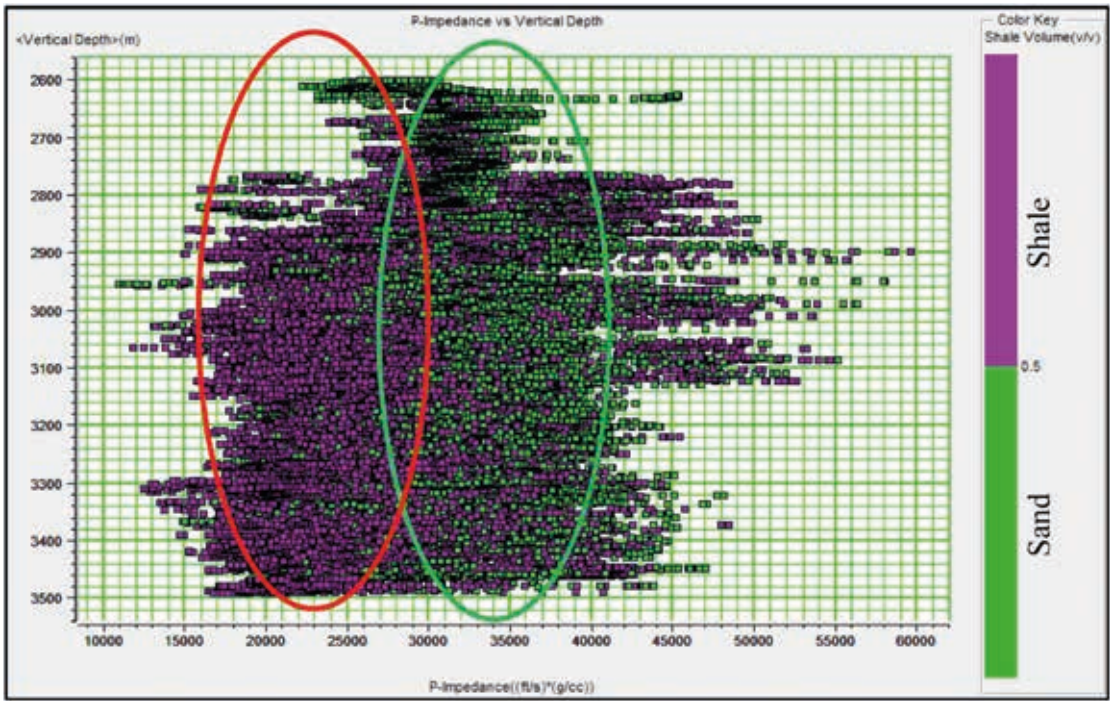

Fig. 4 - P-impedance with depth cross-plot for the AG1 member of the Sufyan oil field. The ellipses indicate the overlapping between shale and sand; colour indicates shale volume.

In the Sufyan oil field, the porosity of AG1 sand is found to be mainly in the range of 10-20%. The sand bodies were vertically set with a range of thickness from 0.6 to 25 m, but dominantly in the 1-5 m (Fig. 5).

There are mainly two types of lithofacies. Table 1 shows the main characteristics of sand and shale in the zones of interest. The data analysis (Table 1 and Fig. 4) indicates that impedance can discriminate between sand and shale in the AG1 member of the Sufyan oil field with some overlap.

Table 1 - Sand and Shale Characteristics of AG1 member of Sufyan Oil Field.

AG1	Cutoff		Density (g/cm^3)	Velocity (m/s)	P-Impedance ($ft/s \times g/cm^3$)
	VSH (%)	VSH (%)			
Shale	50	< 10	2.00 - 2.65	2500 - 4000	15000 - 30000
Sand	50	≥ 10	2.20 - 2.60	3500 - 5000	28000 - 40000

4.2. Inversion analysis

4.2.1. Wavelet extraction and well correlation

The data set used comprises seismic cube of PSTM along with merged logs from 10 wells from the Sufyan oil field. To match the well logs to seismic data, sonic and density logs were used beside tops of formation from both well logs and seismic data by applying time-depth relations and wavelet extraction.

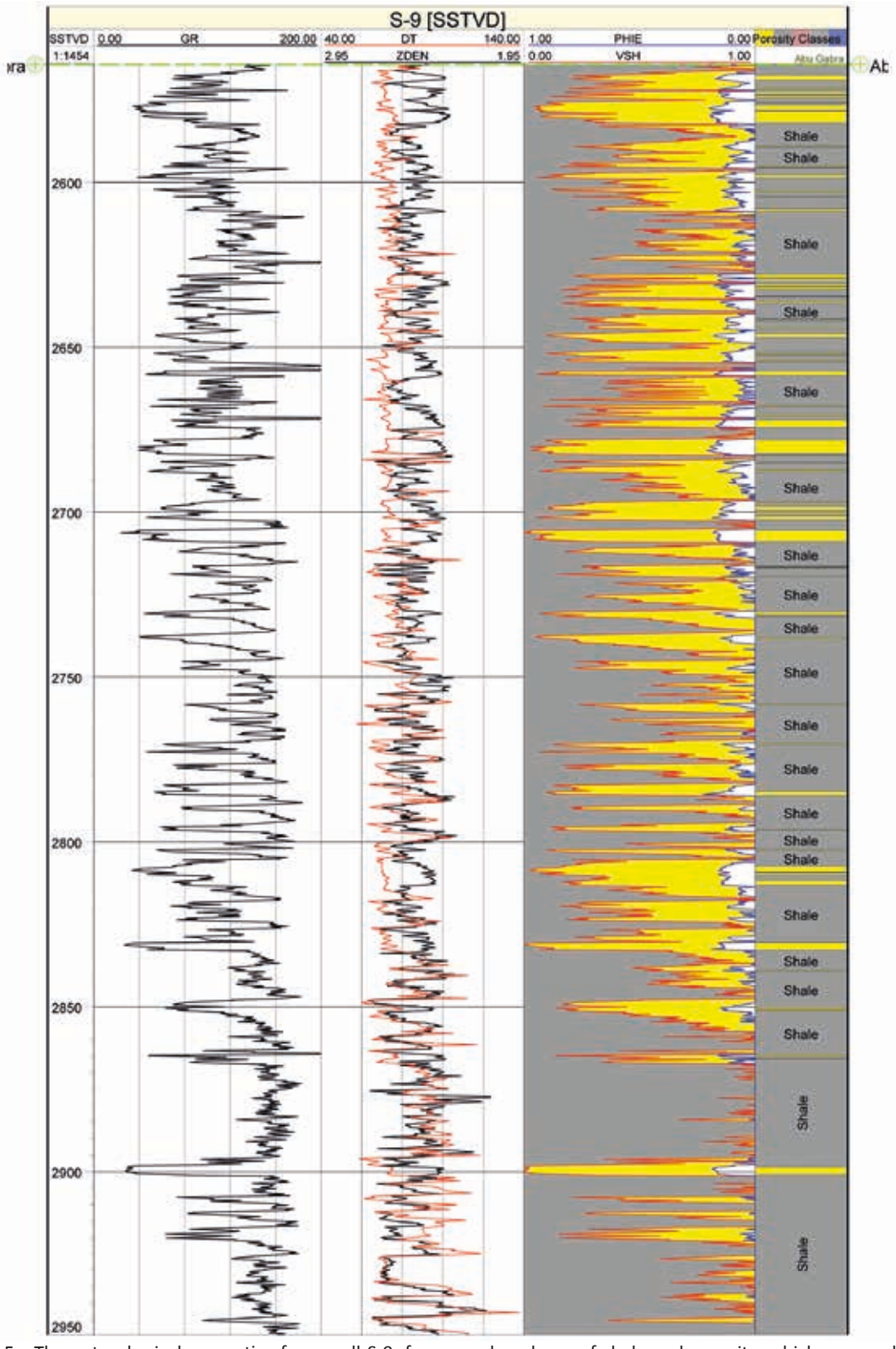

Fig. 5 - The petrophysical properties from well S-9, for example volume of shale and porosity, which are used for lithology classification in the Sufyan oil field and facies discrete logs.

There are two ways for wavelet extraction. One method uses the available well information to extract wavelet components represented in both amplitude and phase. This method requires that the log is already correlated with the seismic traces. The second method uses the seismic data alone to extract wavelet amplitude spectrum. This second method is also called statistical wavelet extraction.

A combination of both methods is used. Firstly, a zero-phase statistical wavelet was extracted with the same amplitude spectrum as the seismic data (Fig. 6a). Then, the log correlation was performed followed by wavelet extraction with the well information (Fig. 6b). From there on, stretching or squeezing is done in an attempt to correlate the synthetic seismogram peaks with the ones obtained from real seismic traces. Consequently, depending on log information and seismic horizons as a guide for the interpolation, the initial model was constructed. Hence, a model of low frequency acoustic impedance is thus acquired using the ten wells to show the pattern of well log impedance value interpolation within the seismic section.

4.2.2. Pre-inversion analysis

The inversion parameters were chosen for BLI, LP-SSI, and MBI methods that give the best estimated R^2 and root mean square (RMS) errors between inverted and actual impedance. If R^2 and RMS errors are within acceptable range, then the entire seismic data is inverted into impedance.

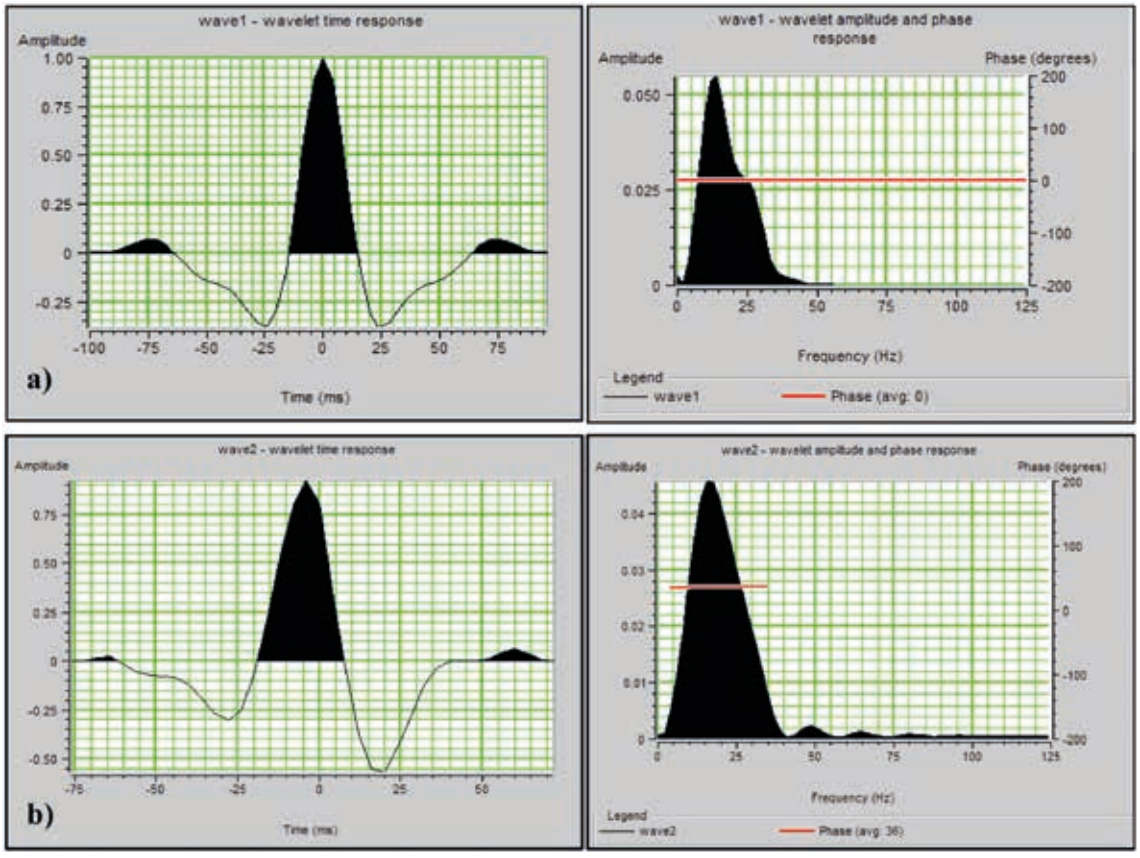

Fig. 6 - Wavelet extraction from Sufyan seismic cube in time and frequency domains: a) zero-phase statistical extracted wavelet using seismic data only; b) extracted wavelet using seismic data and wells used in seismic inversion.

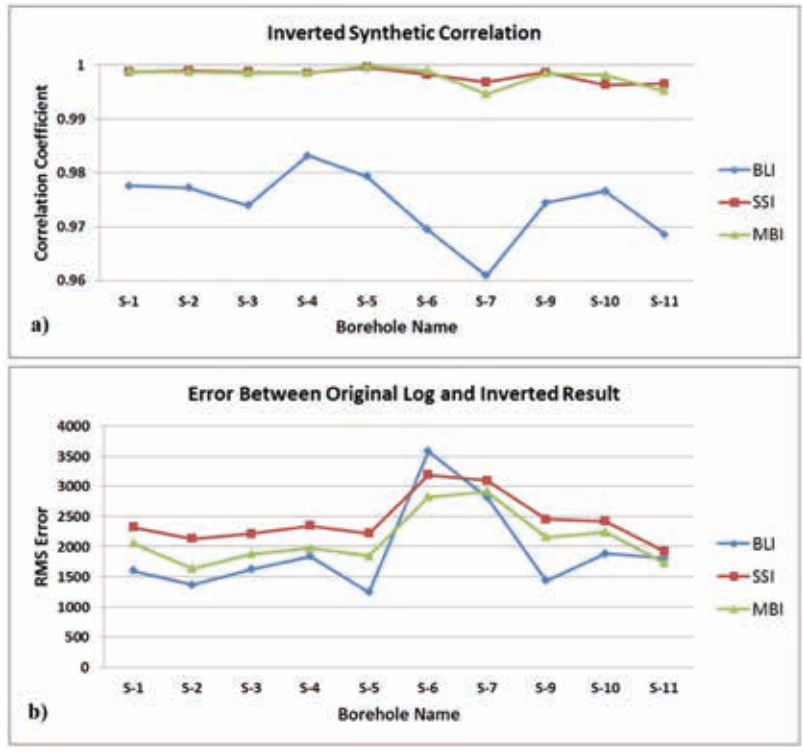

Fig. 7 - Comparison of R^2 (a) and RMS error (b) for all inversion methods.

In BLI, the 'constraint high cut frequency' was applied (Li, 2001; Veeken and Da Silva, 2004). It showed the highest total correlation of 0.973 at frequency of 5 Hz. For LP-SSI, error and correlation values were obtained dependent on 'sparseness and maximum constraint frequency' (Li, 2001; Veeken and Da Silva, 2004), which showed the highest total correlation of 0.998 when sparseness is at 5 and frequency at 5 Hz. The analysis of MBI reveals the superiority of hard constraint to soft-constraint dependent on comparing 'iterations number with constraint error' (Veeken and Da Silva, 2004). It showed that constraint at 30%, has the highest total correlation of 0.998.

In view of the error analysis, the best parameters were chosen and the inversion result at the well locations was compared with the original log. The match between the synthetic and seismic trace gives good values of R^2 in the range between 0.96 and 0.99, (Fig. 7a). Also, RMS errors were estimated (Fig. 7b) which vary from 1240 (ft/s)×(g/cm^3) to 3580 (ft/s)×(g/cm^3).

4.2.3. Inversion results and validation

Subsequent to obtaining an acceptable outcome from the composite traces, the inversion algorithms were applied to the Sufyan 3D seismic data. In addition, the acoustic impedance distribution in-between the location of wells was evaluated. Then, an amplitude spectrum comparison was done between the inverted synthetics of the three inversion algorithms and Sufyan seismic data (Fig. 8d). The figure shows that all spectra follow one another except for the bandlimited inversion with correlation of 0.9815. It also highlights that other algorithms maintain the frequency contents during implementation with correlation of 0.9998 and 0.9994 for LP-SSI and MBI, respectively. Validation was performed by systematically dropping a well completely from the initial model, performing the inversion at that location, and comparing the

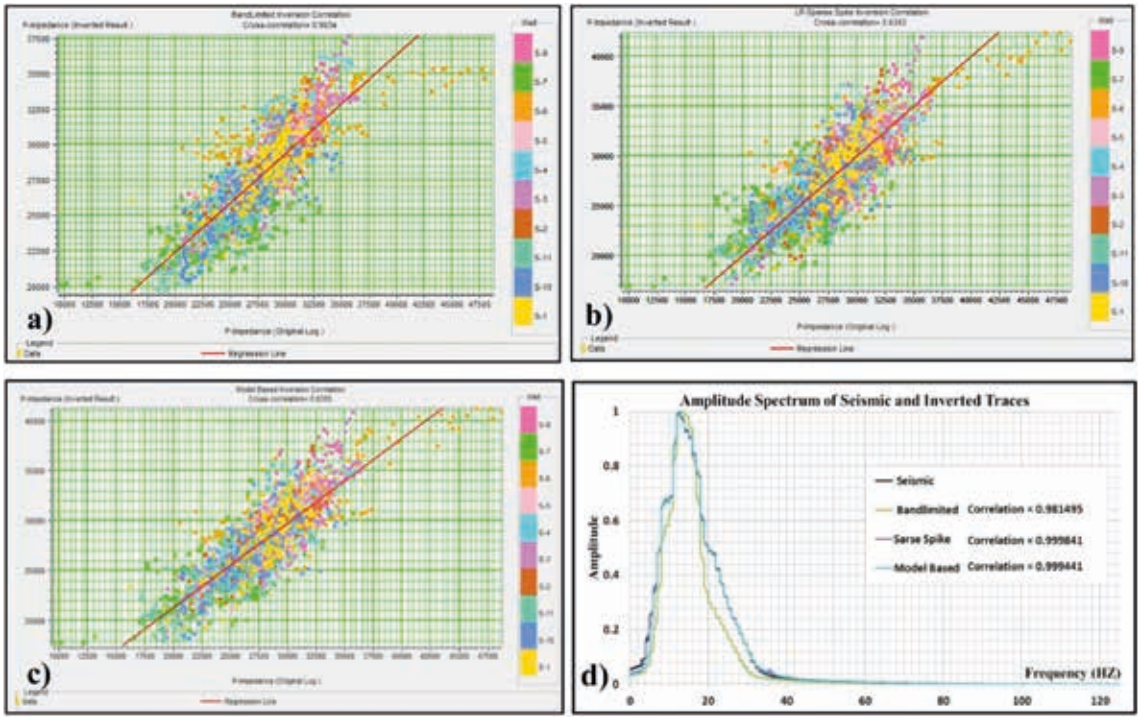

Fig. 8 - Inverted and actual impedance cross-plot for all 10 wells by systematically leaving well out for validation: a) BLI; b) LP-SSI; c) MBI; d) amplitude spectrum correlation comparison of Sufyan oil field between the data of seismic and inverted synthetic traces when the three inversion algorithms are used. The best fit line is represented by the solid red line.

result with the hidden well. Thereafter, the correlation was estimated for the three inversion algorithms for the validation, finding that the BLI and MBI had the highest correlation of 0.95046 and 0.91406, respectively; and the lowest of 0.79957 for LP-SSI (Figs. 8a, 8b, and 8c).

The entire seismic cube of Sufyan was inverted into impedance (Fig. 9). High impedances are clearly visible and highlighted by the ellipses, which may be due to the presence of sand bodies/layers.

Statistical parameters, summarised in Table 2, demonstrate that the MBI is more accurate and produces higher resolution for the Sufyan oil field in comparison with the LP-SSI and BLI cases. The inverted sections show a high impedance anomaly ranging from 33000 to 39000 (ft/s)×(g/cm^3) distributed laterally and vertically with different thicknesses, which may be interpreted as sand bodies/layers.

Table 2 - Summary of quantitative correlation of inversion results.

Parameters	Correlation			RMS Error (ft/s×g/cm^3)
	Impedance		Amplitude Spectrum	
	Training	Validation		
BLI	0.973	0.9505	0.9815	2075.8
LP-SSI	0.988	0.7996	0.9998	1332.7
MBI	0.988	0.9141	0.9994	2174.6

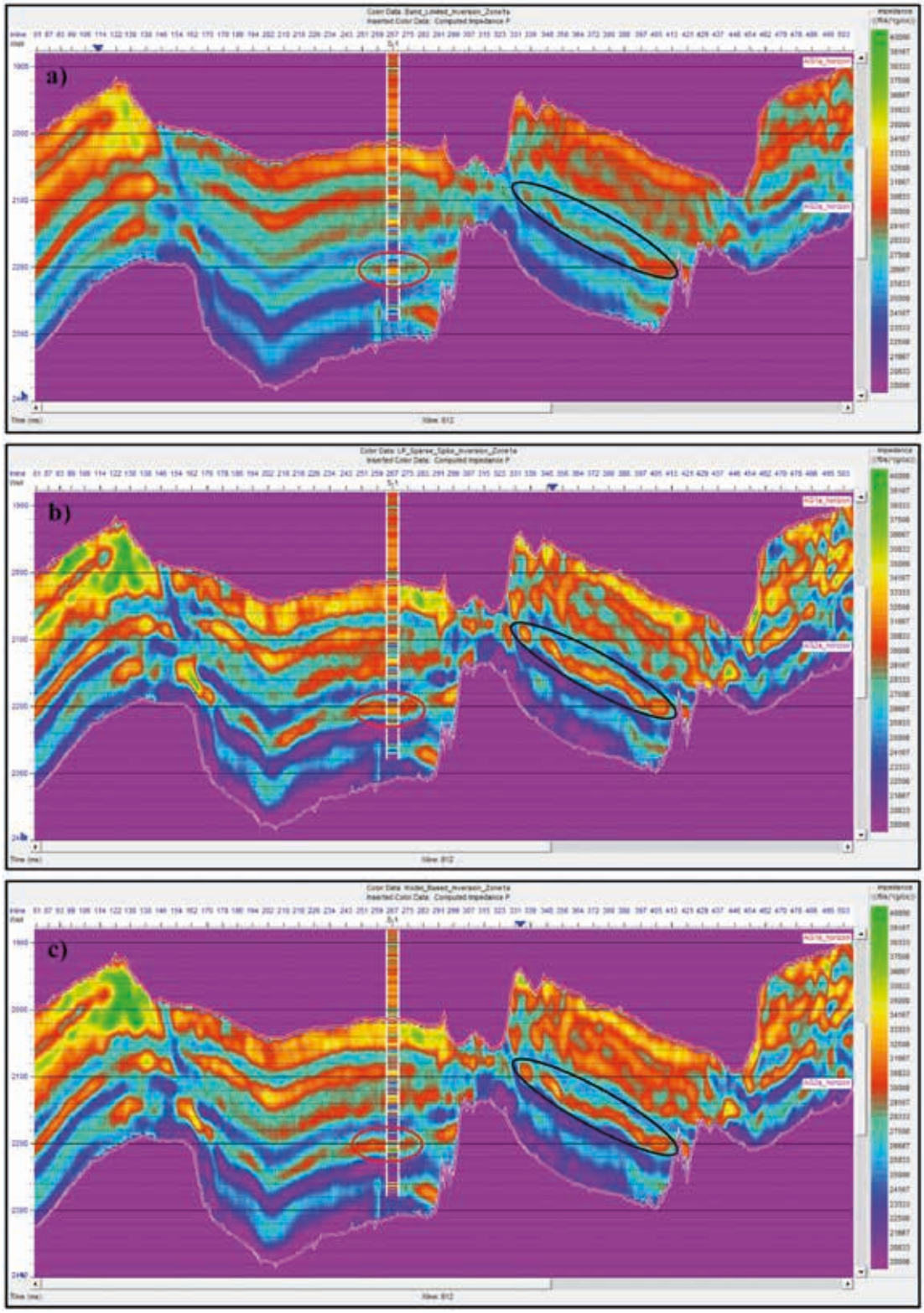

Fig. 9 - Inverted impedance cross-section for x-line 812: a) BLI; b) LP-SSI; c) MBI. The ellipses indicate the good fit between the inversions and well S-1 and the ability of the algorithms to resolve thin beds.

4.3. Porosity estimation

4.3.1. Multi-attribute regression for porosity estimation

Multiple seismic attributes and the porosity of AG1 member relationships were investigated at all well locations. The relationships were extrapolated for the values of porosity away from the wells and the method was performed independently for BLI, LP-SSI and MBI volumes, once used as external attributes. The porosity logs were smoothed to an extreme seismic frequency (45 Hz) to improve correlation results (Fig. 8d).

An extraction of one synthetic trace had been made from the corresponding trace within the 3D volume besides the corresponding inversion results using the average of the ten closest traces around the borehole. The log of the porosity was transformed into time domain and sampled at 4-ms seismic sampling rate.

The attributes were extracted from the seismic volume, visually examined, and narrowed down based on the stepwise linear regression. The analysis using cross-validation reveals that six attributes were used with nine-point convolutional operator when BLI volume is used as the external attribute. Six attributes with five-point convolutional operator used when both LP-SSI and MBI volumes were used as external attributes (Fig. 10).

Table 3 reports the attribute list with its related application (training) errors and validation errors. The multi-attribute regression reveals that the R^2 is 0.8145, 0.7999, and 0.8029 when BLI, LP-SSI, and MBI cubes were used as external attributes, respectively. Also, it reveals RMS difference of 2.1606, 2.2345, and 2.2198, (porosity units in percentage), when BLI, LP-SSI, and MBI cubes were used as external attributes, respectively. The validation test yields R^2 of 0.7155, 0.7229, and 0.7254 with errors of 2.6273, 2.5894, and 2.5799 (porosity units in percentage), when BLI, LP-SSI, and MBI were used, respectively, as external attributes.

The derived relationships at that point were extended to the entire seismic volume (Fig. 11), which shows the x-line 812 cross-section for the AG1 member. Zones of high porosity are obviously distinguished which relate to bodies of sand, while shales relate to low porosity.

The criterion for selecting the final appropriate inversion for reservoir parameter prediction is the validation result. Thus, the external attribute of MBI is the best for porosity prediction when multi-attribute regression is used.

The analysis of multi-attribute so far examines the linear and nonlinear relationship to both of the variables or either of them by fitting a straight line to the transformed data. Neural network is used to derive a relationship that maintains high frequency content of the porosity at the well locations to achieve more enhancements for thin layers.

4.3.2. Neural networks for porosity estimation

An artificial neural network was carried out to enhance the outcome of the multi-linear regression for porosity estimation by evaluating the overall performance of three ANN procedures, namely: MLFN, PNN and RBFN.

Multi-linear regression approach gives a good estimate of the attribute order (Roden *et al.*, 2017), so the attributes in Table 3 were used as the neural system input. For example, six attributes with five-point convolutional operator were chosen when both LP-SSI and MBI volumes are external attributes for porosity prediction. In order to respond to the subsequent enquiry, a good guideline for nodes number is to choose two third of attributes number (Russell, 2004). Therefore, the effective number of attributes is 30 for the above example, hence 20 nodes are used. Lastly, for the number of iterations, a trial and error approach was used for full iterations

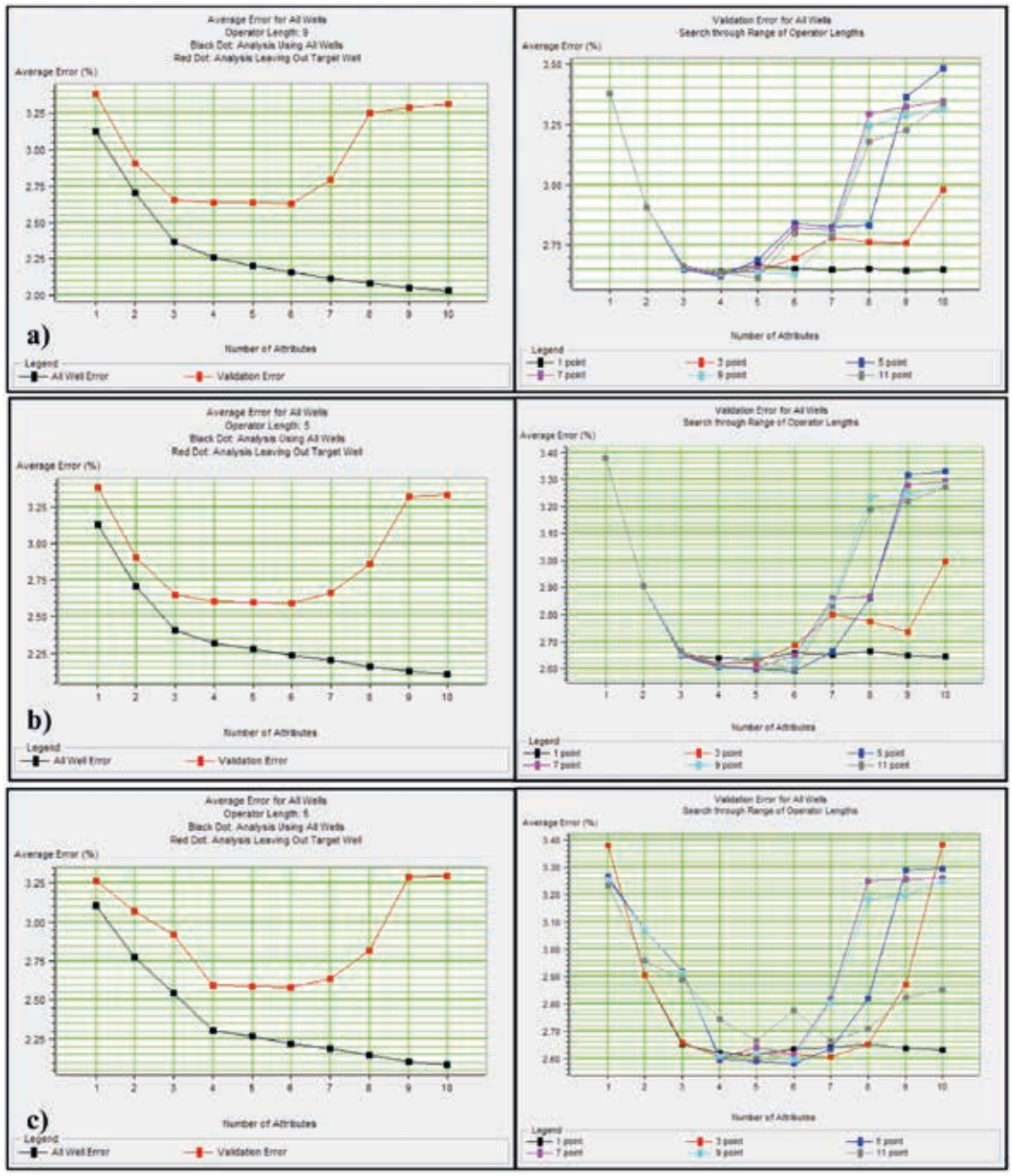

Fig. 10 - The results of stepwise regression and convolutional operator exercise for porosity prediction. The validation error search through six different ranges of operator lengths are on the right. The error plots for training (black dots) and validation (red dots) for the best convolutional operator length combination are on the left. This is when: a) BLI, b) LP-SSI: c) MBI were used as external attributes.

over a range between 10-100 in addition to 100 iterations for conjugate gradient at every full iteration to find the highest validation correlation.

Porosity prediction by MLFN analysis using a trial and error approach, reveals that the total best correlation between predicted porosity and the actual one is achieved when BLI, LP-SSI and

Table 3 - The results of stepwise regression for porosity prediction exercise, when: a) BLI, b) LP-SSI, and c) MBI, were used as external attributes.

No. of Attributes	Final Attribute	Training Error %	Validation Error %
Target = Porosity	**a) Band Limited Inversion**		
1	Time	3.126145	3.381218
2	X-coordinate	2.703318	2.904662
3	Amplitude envelope	2.368178	2.655165
4	(Band Limited Inversion)**2	2.261772	2.632728
5	Dominant frequency	2.203567	2.633938
6	Filter 5/10-15/20	2.160576	2.627338
7	Average frequency	2.114878	2.791952
8	Y-coordinate	2.083687	3.246797
Target = Porosity	**b) LP-Sparse Spike Inversion**		
1	Time	3.126145	3.381203
2	X-coordinate	2.703319	2.904613
3	Amplitude envelope	2.408962	2.646762
4	(LP-Sparse Spike Inversion)**2	2.315518	2.605900
5	Integrate	2.278917	2.597374
6	Filter 15/20-25/30	2.234533	2.589430
7	Dominant frequency	2.202473	2.662933
8	Average frequency	2.159117	2.861777
Target = Porosity	**c) Model Based Inversion**		
1	(Model Based Inversion)**2	3.106778	3.265153
2	Time	2.773688	3.070198
3	Amplitude envelope	2.542323	2.921377
4	X-coordinate	2.301066	2.595218
5	Integrate	2.264598	2.589276
6	Filter 15/20-25/30	2.219761	2.579927
7	Dominant frequency	2.188197	2.634574
8	Average frequency	2.143976	2.819973

MBI were used as external attributes of 0.940, 0.940, and 0.903, with validation correlation of 0.518, 0.711 and 0.679 when using a total iteration of 20, 70, and 60, respectively.

The criterion used for choosing the ultimate acceptable inversion for reservoir parameter prediction is the validation result. Thus, LP-SSI is the best for porosity prediction when MLFN is applied (Table 4). The enhancement of the training correlation results can be observed from 0.799 to 0.940 but R^2 for the result of validation changes from 0.723 to 0.711.

Table 4 presents the summary of the porosity prediction exercise using multi-attribute transform besides artificial neural network methods when different volumes of acoustic impedance were used as external attributes. Also, R^2 of training and validation for all the wells with the corresponding average error in the target unit was presented. The highest validation correlation of the selected method and training correlation are highlighted.

The process of porosity prediction using PNN reveals that the total best correlation between predicted porosity and the actual one when using BLI, LP-SSI and MBI as external attribute is

Table 4 - Porosity prediction exercise summary utilising multi-attribute regression along with artificial intelligence methods. This is when different volumes of acoustic impedance were used as external attributes. The normalised R^2 of training and validation for all the wells with the corresponding average error in target unit (i.e. percentage) are provided. The highest validation correlation (selected method) and training correlation are highlighted.

Method		External Attribute	Validation Result		Application Result	
			Cross-correlation	Error %	Cross-correlation	Error %
Multiple Attribute Regression		BLI	0.7154	2.6273	0.8145	2.16058
		LP-SSI	0.7229	2.5894	0.7999	2.23453
		MBI	0.7254	2.5799	0.8029	2.21976
Neural Network		BLI	0.518034	3.79790	0.940210	1.100927
	MLFN	LP-SSI	0.711093	2.52804	0.939985	1.098257
		MBI	0.678939	2.79153	0.903120	1.383146
		BLI	0.766204	2.07833	0.899111	1.429281
	PNN	LP-SSI	0.799821	1.94044	0.953383	0.998734
		MBI	0.798358	1.94897	0.946918	1.062866
		BLI	0.695586	2.31664	0.975715	0.724376
	RBFN	LP-SSI	0.715199	2.28858	0.986628	0.540571
		MBI	0.705379	2.33067	0.986821	0.536787

0.899, 0.953 and 0.947, with validation correlation of 0.766, 0.799 and 0.798, when global sigma of 1.429, 0.873 and 0.813 is used, respectively.

For porosity prediction using RBFN, adopting a trial and error approach, the best correlation between predicted porosity and the actual one was obtained when BLI, LP-SSI and MBI are used as external attribute of 0.976, 0.987 and 0.987, with validation correlation of 0.696, 0.715 and 0.705, respectively, when sigma of 1.0 is used.

The external attribute of LP-SSI is likewise the best for porosity prediction using RBFN, MLFN and PNN (Table 4).

Fig. 12 shows porosity cross-section of the x-line 812 of the AG1 member when: a) MLFN, b) PNN, and c) RBFN were used as prediction tool, and LP-SSI as external attribute. The derived ANN transforms have a good fit to the well log, in addition to extra detail that is seen in the MLFN, when compared to the PNN and RBFN.

The artificial neural network approach demonstrated that higher-frequency outcomes can be created and clearly related to thin sand bodies/layers (high porosity value). Namely, MLFN approach is the best for reservoir prediction rather than PNN or RBFN, even when the latter has higher R^2.

4.4. Vertical resolution estimation

Seismic resolution is the capability to recognise two features from each other. Vertical and horizontal resolutions are the types of seismic resolution. Vertical resolution decides the thickness of the beds and clarifies the distance between two interfaces as isolated reflectors.

Widess (1973) wrote about the threshold for resolution; Kallweit and Wood (1982) define the acceptable threshold for vertical seismic resolution as around $\lambda/8$ and $\lambda/4$, respectively; where λ is the dominant wavelength. Mora *et al.* (2020) used an integration of multi-attribute transform and bandwidth extension to enhance the prediction quality incorporated in the property prediction accuracy and vertical resolution improvement.

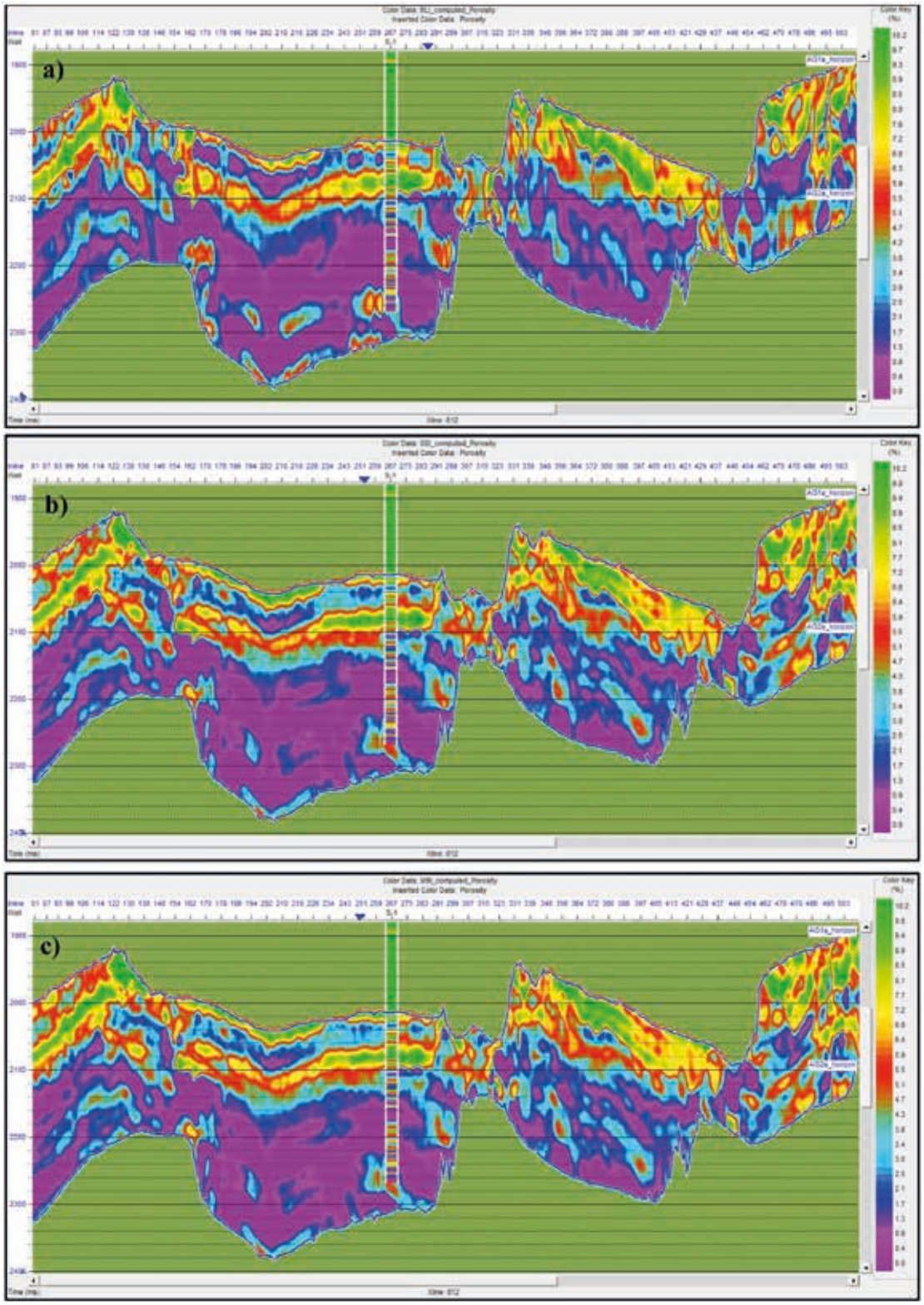

Fig. 11 - Cross-sections of the porosity distribution in time domain of x-line 812 when external attributes are: a) BLI, b) LP-SSI; c) MBI. The embedded colour log is the target porosity log at this location.

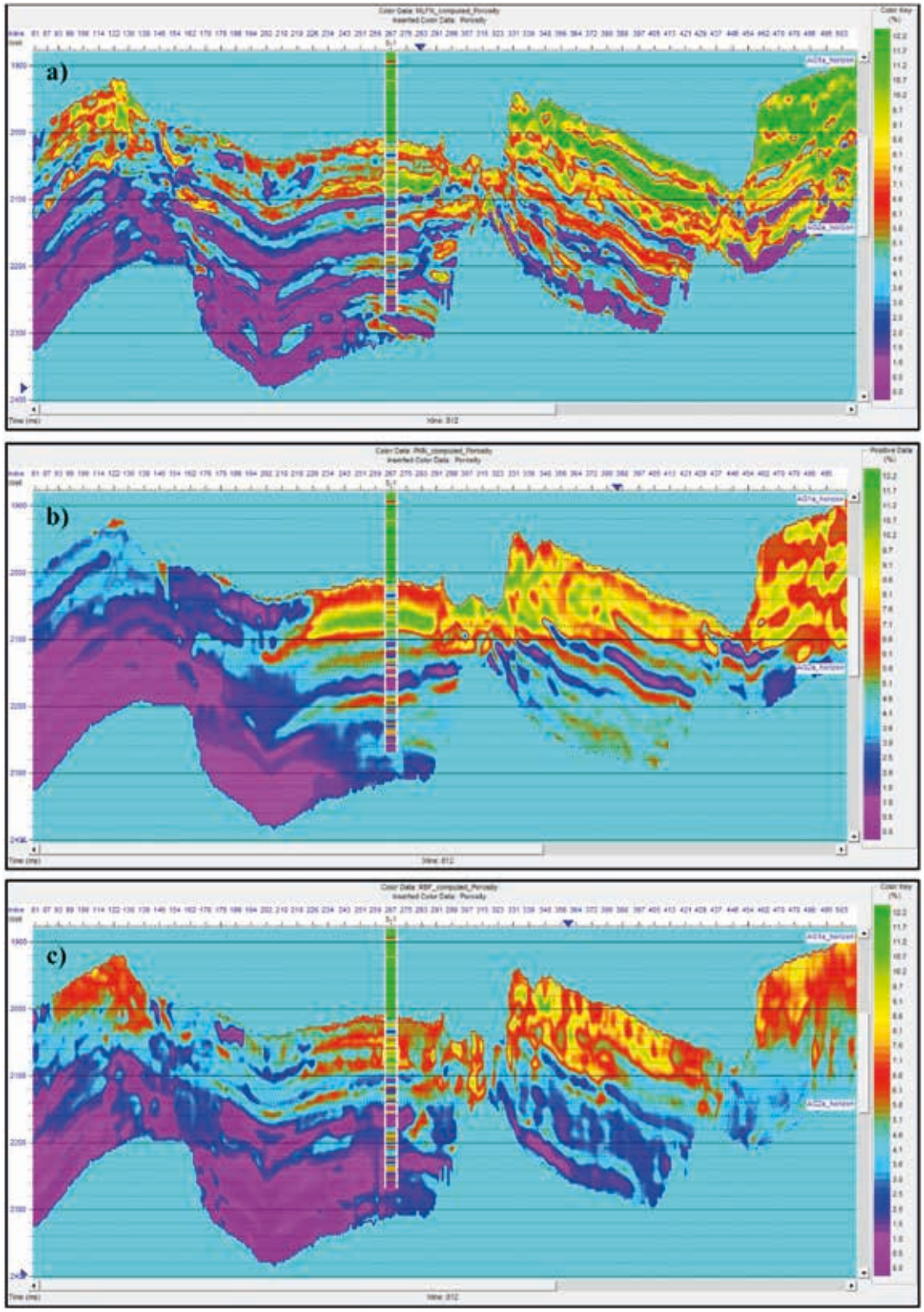

Fig. 12 - The predicted porosity distribution cross-sections in time domain of x-line 812 when LP-SSI is used as external attribute; using: a) MLFN, b) PNN; c) RBFN. The embedded colour log is the target porosity log at this location.

The seismic data analysis for the Sufyan oil field indicates a vertical seismic resolution of approximately 23.5-47 m, when sonic logs average velocity of the AG1 member interval is used (3758 m/s), along with using amplitude spectrum to determine dominant frequency (f = 20 Hz). However, sand bodies that were identified from well logs are vertically distributed with average thickness ranging from 0.6 m to 25 m, but mainly in the 1-5 m.

Several thin sand layers were recognised using available logs. A single well is shown in Fig. 12i, which displays shale volume and porosity logs, in which the low shale volume (≤50%) and high porosity (≥10%) suggest porous clean sandstone in specified zones. The first zone has a thickness of 10 m and the second zone has a thickness of 7 m, which are both below the seismic resolution threshold. On porosity prediction using PNN and RBFN, neither layer is recognised but the 10-m layer interval is still recognised on the porosity prediction using MLFN. In the 7-m zone, the layer is not recognised. Another example is shown in Fig. 12ii, where one interval of 13 m is clearly detected after using MLFN and RBFN. This is almost undetectable in PNN analysis.

5. Discussion

Three algorithms of post-stack acoustic impedance inversion were used. All post-stack acoustic impedance inversion (BLI, LP-SSI, and MBI) results are closely related. The synthetic and seismic trace comparison shows good values of R^2 that vary from 0.96 to 0.99. Also, RMS average variations were estimated which vary from 1300 (ft/s)×(g/cm^3) to 2200 (ft/s)×(g/cm^3).

Statistical parameters summarised in Table 2, demonstrate that the MBI is more accurate and produces higher resolution acoustic impedance for the Sufyan oil field in comparison with the LP-SSI and BLI cases. The inverted sections show a high impedance anomaly ranging from 33,000 to 39,000 (ft/s)×(g/cm^3) distributed laterally and vertically with different thicknesses, which may be interpreted as sand bodies/layers.

Porosity was predicted using multi-attribute transform and neural networks in the selected reservoir using stepwise regression to find appropriate seismic attributes (Table 3). A comparative analysis for porosity estimation was carried out using each of the individual inversion algorithms previously obtained with three different techniques of neural network (i.e. MLFN, PNN, and RBFN). Nine correlations have been found; three correlations for each seismic inversion volume when MLFN, PNN, and RBFN were applied for porosity estimation in the area of the study using well-log and 3D seismic data (Table 4). The results show that using MLFN with the combination of LP-SSI (0.711 validation error) shows extra details and good lateral continuity throughout the sections (Figs. 12 and 13).

This case study has demonstrated that higher-frequency outcomes can be created and clearly related to thin sand bodies (high porosity value) when the MLFN with LP-SSI approach is used for reservoir prediction. It achieved better outcomes than with PNN or RBFN, even when the latter has higher R^2 (Fig. 13). This also indicates that the LP-SSI is more accurate for prediction of petrophysical parameters for Sufyan oil field seismic data when neural networks are used, compared to other inversion techniques.

This methodology has been demonstrated on a set of 10 wells log data. Hence, poor distribution and unreliable well logs may give rise to an inaccurate wavelet extraction and, therefore, affect the entire processing sequence of prediction. Thus, increasing the number of wells may enhance the reliability of prediction results.

Accurate and quantitative prediction of the distribution and properties of thin-beds is a

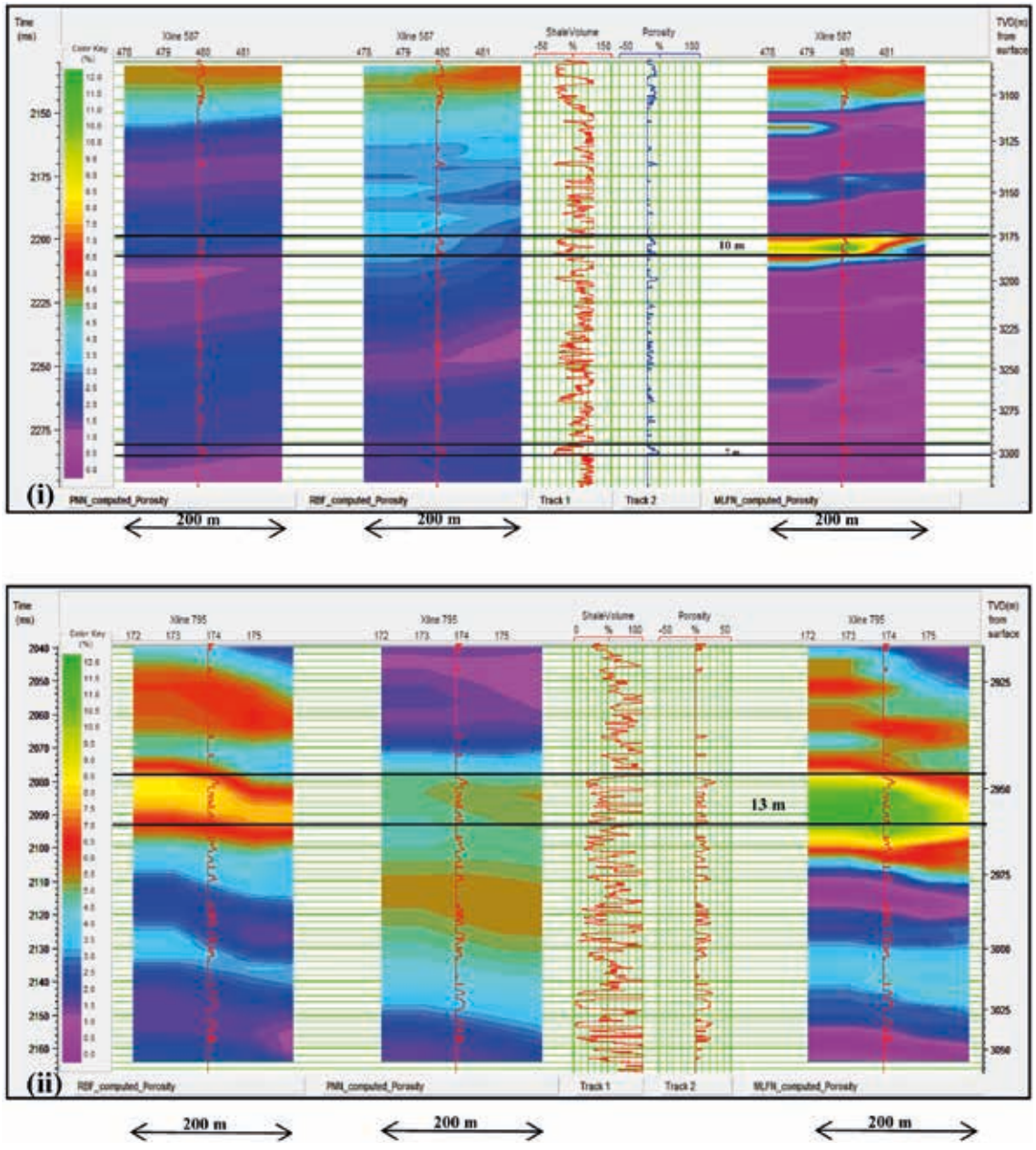

Fig. 13 - Porosity, shale volume logs and porosity volumes produced using MLFN (right), RBFN and PNN (left) volumes for: i) well S-10 and ii) well S-11. Thin zones of interest highlighted by black lines. Porosity log curves are embedded.

significant challenge, characterised by considerably raised non-uniqueness and lack of certainty compared to the characteristics of thick reservoirs. Thus, studying more cases can achieve improved thin-bed prediction.

6. Conclusions

A comparative analysis of three types of post-stack inversion techniques has been carried out. The extracted variety of seismic attributes and porosity using these inversion techniques is meant to examine whether integration of multi-attribute analysis and neural networks could bring about better clarification of layers below the seismic resolution threshold. The resulting resolution and precision of multi-attribute rock properties prediction were compared using MLFN, PNN, and RBFN to predict porosity within the Sufyan oil field, Muglad rift basin, Sudan. From the study, it can be concluded that:

- the results (Table 2) show that BLI, LP-SSI, and MBI techniques give good and mutually consistent results with high-impedance anomaly extending from 33,000 to 39,000 (ft/s)×(g/cm^3), distributed laterally and vertically, with different thicknesses zones corresponding to the target sand bodies/layers. However, MBI is considered the best for Sufyan seismic data based on validation error and amplitude spectrum correlation;
- as referenced in Table 3, by using a proper integration of seismic attributes for driving porosity, multi-attribute regression revealed that the external attribute of MBI is the best for porosity prediction with training correlation of 0.8029;
- three different types of neural networks (MLFN, PNN, and RBFN) were used for subsequent prediction of porosity (Table 4). The PNN shows that linear programming sparse spike inversion (LP-SSI) has the highest training correlation of 0.9534, when used as an external attribute;
- however, MLFN shows that LP-SSI, when used as an external attribute, is more precise and delivers high-resolution images compared with those estimated with other combinations with training correlation of 0.9400;
- the study reveals that using the combination of LP-SSI and MLFN approaches enhances the prediction goodness regarding property prediction reliability and resolution. This applies to the vertical resolution, which respects a superior conception of the field in terms of defining unseen layers of interest;
- the use of only 10 wells could be a limitation for the computational approaches adopted. Thus, increasing the number of wells may enhance the predicting results reliability.

As an overall conclusion, the outcome suggests that the integration of LP-SSI and MLFN processes with each other can produce reliable results of petrophysical properties of the subsurface and improve thin layer resolution in such reservoirs. Additionally, the proposed methodology can minimise risks of drilling along with enhancing the rate of success at the initial phase of reservoir evaluation. Moreover, it can give an appropriate volume of porosity data that can be used in building reservoir geological models during the reservoir development phase.

Acknowledgments. Thanks are due to the Ministry of Petroleum Republic of Sudan for providing the data sets for use in this research and granting the publication of this study. We also thank A.G. Farwa, A.R.O. Mohamed, University of Khartoum and W.K. Shuaib for their review and comments.

REFERENCES

Brown A.R.; 1996: *Seismic attributes and their classification*. The Leading Edge, 15, 1090, doi: 10.1190/1.1437208.

Brown A.R.; 2001: *Understanding seismic attributes*. Geophys., 66, 47-48.

Carcione J.M., Gei D., Picotti S., Misnan M.S., Rashidi M., Bakar Z.A.A., Harith Z.Z.T., Bahri N.H.S. and Hashim N.; 2020: *Porosity and permeability of the overburden from wireline logs: a case study from offshore Malaysia*. Geomech. Geophys. for Geo-Energy and Geo-Resour., 6, 1-12.

Cole J.M., Abdelrahim O.B., Hunter A.W., Schrank E. and Ismail M.S.B.; 2017: *Late Cretaceous spore-pollen zonation of the Central African Rift System (CARS), Kaikang trough, Muglad basin, south Sudan: angiosperm spread and links to the Elaterates province*. Palynol., 41, 547-578.

Dresser Atlas; 1979*: Log interpretation charts*. Dresser Industries Inc., Houston, TX, USA, 108 pp.

Eftekharifar M. and Han D.H.; 2011: *3D Petrophysical modeling using complex seismic attributes and limited well log data*. In: Expanded Abstracts, 81st SEG Annual Meeting, Society of Exploration Geophysicists, San Antonio, TX, USA, pp. 1887-1891.

Eskandari H., Rezaee M.R. and Mohammadnia M.; 2004: *Application of multiple regression and artificial neural network techniques to predict shear wave velocity from wireline log data for a carbonate reservoir south-west Iran*. Canad. Soc. Explor. Geophys. Recorder, 29, 42-48.

Fairhead J.D.; 1988: *Mesozoic plate tectonic reconstructions of the central south Atlantic Ocean: the role of the west and central African rift system*. Tectonophys., 155, 181-191.

Ferguson R.J. and Margrave G.F.; 1996: *A simple algorithm for band-limited impedance inversion*. CREWES Res. Rep., 8, 1-10.

Gastaldi C., Biguenet J.P. and De Pazzis L.; 1997: *Reservoir characterization from seismic attributes: an example from the Peciko field (Indonesia)*. The Leading Edge, 16, 263-266.

Hampson D.P., Schuelke J.S. and Quirein J.A.; 2001: *Use of multiattribute transforms to predict log properties from seismic data*. Geophys., 66, 220-236.

Hou Q., Zhu J. and Lin B.; 2016: *Estimation of reservoir porosity using probabilistic neural network and seismic attributes*. Global Geol., 19, 6-12.

Kallweit R.S. and Wood L.C.; 1982: *The limits of resolution of zero-phase wavelets*. Geophys., 47, 1035-1046.

Kaska H.V.; 1989: *A spore and pollen zonation of Early Cretaceous to Tertiary nonmarine sediments of central Sudan*. Palynol., 13, 79-90.

Khoshdel H. and Riahi M.A.; 2011: *Multi attribute transform and neural network in porosity estimation of an offshore oil field - A case study*. J. Pet. Sci. Eng., 78, 740-747.

Larionov V.V.; 1969: *Radiometry of boreholes*. Nedra, Moscow, U.S.S.R., 127 pp.

Li Q.; 2001: *LP sparse spike inversion*. Strata Technique Document, Hampson-Russell Software Services Ltd., Calgary, AB, CA, 14 pp.

Lirong D., Dingsheng C., Zhi L., Zhiwei Z. and Jingchun W.; 2013: *Petroleum geology of the Fula sub-basin, Muglad basin, Sudan*. J. Pet. Geol., 36, 43-59.

Makeen Y.M., Abdullah W.H., Hakimi M.H. and Elhassan O.M.; 2015a: *Organic geochemical characteristics of the Lower Cretaceous Abu Gabra Formation in the great Moga oilfield, Muglad basin, Sudan: implications for depositional environment and oil-generation potential*. J. Afr. Earth Sci., 103, 102-112.

Makeen Y.M., Abdullah W.H., Hakimi M.H., Hadad Y.T., Elhassan O.M. and Mustapha K.A.; 2015b: *Geochemical characteristics of crude oils, their asphaltene and related organic matter source inputs from Fula oilfields in the Muglad basin, Sudan*. Mar. Pet. Geol., 67, 816-828.

Makeen Y.M., Abdullah W.H., Hakimi M.H. and Mustapha, K.A.; 2015c: *Source rock characteristics of the Lower Cretaceous Abu Gabra Formation in the Muglad basin, Sudan, and its relevance to oil generation studies*. Mar. Pet. Geol., 59, 505-516.

Makeen Y.M., Abdullah W.H., Ayinla H.A., Hakimi M.H. and Sia S.G.; 2016: *Sedimentology, diagenesis and reservoir quality of the Upper Abu Gabra Formation sandstones in the Fula sub-basin, Muglad basin, Sudan*. Mar. Pet. Geol., 77, 1227-1242.

Maurya S.P. and Sarkar P.; 2016: *Comparison of post stack seismic inversion methods: a case study from Blackfoot field, Canada*. Int. J. Sci. Eng. Res., 7, 1091-1101.

Maurya S.P. and Singh K.H.; 2015: *LP and ML sparse spike inversion for reservoir characterization - A case study from Blackfoot area, Alberta, Canada*. In: Proc. 77th EAGE Conference and Exhibition 2015, Madrid, Spain, Vol. 1, pp. 1-5, doi: 10.3997/2214-4609.201412822.

Maurya S.P. and Singh N.P.; 2018: *Application of LP and ML sparse spike inversion with probabilistic neural network to classify reservoir facies distribution - A case study from the Blackfoot field, Canada*. J. Appl. Geophys., 159, 511-521.

Maurya S.P. and Singh, N.P.; 2019: *Estimating reservoir zone from seismic reflection data using maximum-likelihood sparse spike inversion technique: a case study from the Blackfoot field (Alberta, Canada)*. J. Pet. Explor. Prod. Technol., 9, 1907-1918.

McHargue T.R., Heidrick T.L. and Livingston J.E.; 1992: *Tectonostratigraphic development of the interior Sudan rifts, central Africa*. Tectonophys., 213, 187-202.

Mora D., Castagna J., Meza R., Chen S. and Jiang R.; 2020: *Case study: seismic resolution and reservoir characterization of thin sands using multiattribute analysis and bandwidth extension in the Daqing field, China*. Interpretation, 8, T89-T102.

Pandey Y.N., Rastogi A., Kainkaryam S., Bhattacharya S. and Saputelli L.; 2020: *Machine learning in the oil and gas industry*. Apress, Berkeley, CA, USA, 320 pp., doi: 10.1007/978-1-4842-6094-4.

Pavanel E., Fervari M., Corrao A., Gallagher M. and Ciurlo B.; 2009: *Pay sand mapping using seismic multi-attribute calibration proved to be effective from development to near field exploration stages: a case study from De Soto Canyon, Gulf of Mexico*. In: Paper presented at 79th SEG Annual Meeting, Society of Exploration Geophysicists, Houston, TX, USA, SEG-2009-0567.

Roden R., Smith T.A., Santogrossi P., Sacrey D. and Jones G.; 2017: *Seismic interpretation below tuning with multiattribute analysis*. The Leading Edge, 36, 330-339.

Russell B.H.; 1988: *Introduction to seismic inversion methods (No. 2).* Society of Exploration Geophysicists Books, Houston, TX, USA, 178 pp., doi: 10.1190/1.9781560802303.

Russell B.H.; 2004: *The application of multivariate statistics and neural networks to the prediction of reservoir parameters using seismic attributes.* Ph.D. Thesis in Philosophy, Department of Geology and Geophysics, University of Calgary, Calgary, AB, Canada, 391 pp.

Russell B. and Hampson D.; 1991: *Comparison of poststack seismic inversion methods*. In: Expanded Abstracts 61st SEG Annual Meeting, Society of Exploration Geophysicists, Houston, TX, USA, pp. 876-878, doi: 10.1190/1.1888870.

Sacchi M.D. and Ulrych T.J.; 1995: *High-resolution velocity gathers and offset space reconstruction*. Geophys., 60, 1169-1177.

Schlumberger; 1987: *Log interpretation principles/applications*. Schlumberger Ltd., Houston, TX, USA, 198 pp.

Schull T.J.; 1988: *Rift basins of interior Sudan: petroleum exploration and discovery*. Am. Assoc. Pet. Geol. Bull., 72, 1128-1142.

Shuaib M.E.K.; 2013: *Seismic attributes and petrophysical modeling of the Aradeiba-D member, Muglad rift basin, Sudan.* M. Sc. Thesis in Geophysical Sciences, King Fahd University of Petroleum and Minerals, Dhahran, Saudi Arabia, 146 pp.

Simm R.; 2009: *Simple net pay estimation from seismic: a modelling study*. First Break, 27, 45-53, doi: 10.3997/1365-2397.2009014.

Sukmono S.; 2007: *Application of multi-attribute analysis in mapping lithology and porosity in the Pematang-Sihapas groups of central Sumatra basin, Indonesia*. The Leading Edge, 26, 126-131.

Taner M.T., Koehler F. and Sheriff R.E.; 1979: *Complex seismic trace analysis*. Geophys., 44, 1041-1063.

Tong X., Dou L., Tian Z., Pan X. and Zhu X.; 2004: *Geological mode and hydrocarbon accumulation mode in Muglad passive rift basin of Sudan*. Acta Pet. Sin., 25, 19-24.

Veeken P.C.H. and Da Silva A.M.; 2004: *Seismic inversion methods and some of their constraints*. First Break, 22, 47-70, doi: 10.3997/1365-2397.2004011.

Waters K.H.; 1978: *Reflection seismology*. John Wiley and Sons, New York, NY, USA, 390 pp.

Widess M.B.; 1973: *How thin is a thin bed?*. Geophys., 38, 1176-1180.

Wu D., Zhu X., Su Y., Li Y., Li Z., Zhou Y. and Zhang M.; 2015: *Tectono-sequence stratigraphic analysis of the lower cretaceous Abu Gabra Formation in the Fula sub-basin, Muglad basin, southern Sudan*. Mar. Pet. Geol., 67, 286-306.

Yassin M.A., Hariri M.M., Abdullatif O.M., Korvin G. and Makkawi M.; 2017: *Evolution history of transtensional pull-apart, oblique rift basin and its implication on hydrocarbon exploration: a case study from Sufyan sub-basin, Muglad basin, Sudan*. Mar. Pet. Geol., 79, 282-299.

Yassin M.A., Hariri M.M., Abdullatif O.M., Makkawi M., Bertotti G. and Kaminski M.A.; 2018: *Sedimentologic and reservoir characteristics under a tectono-sequence stratigraphic framework: a case study from the Early Cretaceous, Upper Abu Gabra sandstones, Sufyan sub-basin, Muglad basin, Sudan*. J. Afr. Earth Sci., 142, 22-43.

Zahmatkesh I., Kadkhodaie A., Soleimani B., Golalzadeh A. and Azarpour M.; 2018: *Estimating Vsand and reservoir properties from seismic attributes and acoustic impedance inversion: a case study from the Mansuri oilfield, SW Iran*. J. Pet. Sci. Eng., 161, 259-274.

Zhou H.W.; 2014: *Practical seismic data analysis*. Cambridge University Press, Cambridge, UK, 496 pp.

Corresponding author: Migdad ElKheir Shuaib
Department of Geology, Faculty of Science, University of Khartoum
P.O. Box: 123, 11115 Khartoum, Sudan
Phone: +249912183139, e-mail: migdadshuaib@yahoo.com